

Optimization of Contrast-Enhanced Digital Breast Tomosynthesis

Ann-Katherine Carton, Jingjing Li, Sara Chen, Emily Conant,
and Andrew D.A. Maidment

University of Pennsylvania, Department of Radiology,
3400 Spruce Street, Philadelphia, PA, USA, 19104
{ann-katherine.carton, sara.chen, emily.conant,
andrew.maidment}@uphs.upenn.edu

Abstract. Digital breast tomosynthesis (DBT) is a tomographic technique in which individual slices through the breast are reconstructed from x-ray projection images acquired over a limited angular range. In contrast-enhanced DBT (CE-DBT) functional information is observed by administration of a radiographic contrast agent. The uptake of iodine in the breast is very small and causes changes in x-ray transmission that are smaller than 5%. This presents significant technical challenges if quantitative assessment of contrast agent concentration in tissue is desired. We modeled CE-DBT acquisition by simulating x-ray spectra from 40 to 49 kV. Comparison of attenuation data of our simulated and measured spectra were found to agree well. We investigated the effect of patient motion and scatter on iodine uptake. These parameters were evaluated by means of experiments and theoretical modeling.

1 Background

Digital breast tomosynthesis (DBT) is a tomographic technique for imaging the breast morphology at a dose comparable to digital mammography. However, as breast tumor growth and metastasis are accompanied by neoangiogenesis, a functional tomographic imaging technique is desired. Contrast-enhanced digital breast tomosynthesis (CE-DBT) [1] would potentially integrate the benefits of both CE digital mammography [2, 3] and DBT [4-7]; thus, providing both functional information and improved breast cancer morphology by minimizing the superimposition of nonadjacent breast tissues that occurs with projection mammograms. Temporal analysis of contrast enhancement may further help to distinguish benign and malignant lesions.

The uptake of iodine in the breast is very small and thus causes only small changes in x-ray transmission; typically less than 5%. This presents significant technical challenges if quantitative assessment of contrast agent uptake is desired [1]. Technical factors that significantly influence quantitative analysis of CE-DBT exams are exposure reproducibility, linearity of the detector as a function of position, temporal response of the detector, scatter and patient motion. In this paper, we will discuss scatter, and patient motion.

2 Methods

We have used a modified GE 2000D under IRB approval to gain initial experience in CE-DBT. In the experiments described, we have used temporal subtraction. High energy images are acquired before and after administration of an iodinated contrast agent. Logarithmic subtraction of these images is then performed. The signal intensities (SI) of the resulting images are proportionally to the uptake of iodine.

2.1 Spectrum

To model the acquisition process, x-ray spectra in the range of 40 to 49 kV were simulated by extrapolating Boone's model [8]. We validated our simulations using a least-squares comparison (χ^2 values) between attenuation data from our simulated spectra and attenuation data measured with the GE Senographe 2000D. We used high-purity Al filters to determine the attenuation curves. Minimum χ^2 values were found by adjusting the kV ($kV_{\text{equivalent}}$) and adding or subtracting Al ($Al_{\text{equivalent}}$) to the simulated spectra. We also compared the half value layers (HVL) and quarter value layers (QVL) of the simulations and the measurements. In this paper, we compare simulated and measured attenuation data from a Mo-target with 1 mm Al filtration, and a Rh-target with 0.27 mm Cu filtration.

2.2 Scatter

We performed CE-DBT without a grid. Scatter, S , was estimated by extrapolation of signal intensity measurements under Pb-disks with diameters of 3.9 to 23 mm to a disk of zero diameter. Scatter fractions (SF) were then calculated as the fraction of S to the SI value in the open field at the same position, which consist of S and primary radiation, P . These measurements were repeated as a function of position in 50% glandular-50% adipose breast equivalent phantoms (CIRS, Norfolk, VA), and various breast equivalent thickness. The phantoms were positioned so as to mimic the MLO breast position, including higher order scatter from the chest. A 49 kV spectrum with a 0.27 mm Cu filter was applied.

As part of our clinical CE-DBT trial, we have measured SF in the MLO projection images of 6 patients. Pb-disks 12 mm in diameter were positioned on top of the compression plate while the breast was compressed and a series of projection images was acquired over a 50° arc (as measured at the fulcrum, 20 cm above the breast support). SF were then calculated from the SI measured in the shadows of the Pb-disks, giving S , and the SI was also measured at the same position in the previously acquired pre-contrast projection images, thus giving $P + S$. The SF in the clinical data were compared with the SF calculated from the 12 mm Pb-disks in the phantom images. The same mammography unit and spectrum were used as in the phantom measurements.

We modeled the effect of scatter on the quantification of the iodine concentration for various breast thicknesses. We simulated a Senographe 2000D tube operated at 49 kV with a Rh target and 0.27 mm Cu filtration. Our simulation includes the attenuation of the Be-window, Cu-filter, compression plate, air, ICRU-44 breast tissue, and the CsI detector material. We used the SF measured near the center of the breast equivalent phantoms. We calculated the contrast as a function of iodine uptake for the various breast thicknesses and then calculated the error in the iodine concentration estimate due to the scatter.

2.3 Patient Motion

In temporal subtraction, pre- and post-contrast images are subtracted. Any breast motion between series will result in artifacts and an erroneous estimate of the iodine uptake will be calculated. In our clinical trial, the total acquisition time could exceed 10 minutes, depending on the experimental protocol. Thus, breast motion is inevitable.

We developed a measure to demonstrate the effect of breast motion on the estimated iodine uptake. In 12 patient images, we selected ROIs where the breast thickness was constant. The relative SI variations, corrected for scatter by using measured SF, were calculated between pixel positions that are Δx apart from each other. We varied Δx from 1 to 128 pixels (0.1 - 12.8 mm). These measurements were calculated for displacements in the horizontal and vertical direction. The relative SI variations were related to corresponding iodine concentrations using our simulation. These simulations considered a Senographe 2000D x-ray tube operated at 49 kV with a Rh-target and 0.27 mm Cu filtration. The simulation includes the attenuation of the Be-window, Cu-filter, compression plate, air, ICRU-44 breast tissue, and the CsI detector material.

3 Results

3.1 Spectrum

A comparison of the simulated and measured attenuation data are presented in Tables 1 and 2. The measured attenuation data in Table 1 are from a GE Senographe 2000D operated with a Rh-target and 0.27 mm Cu filtration. The tube has a 0.69 mm Be window, and a 2 mm compression plate was in the x-ray beam. The measured attenuation data in Table 2 are from a GE DMR. The Mo-target x-ray source was used with 1 mm Al filtration. The x-ray tube window was composed of 0.69 mm thick Be and a 2 mm compression plate was again in place.

Table 1. Comparison of the measured and simulated attenuation data for a Rh-target tube filtered with 0.27 mm Cu

nominal kV	kV _{equivalent}	Al _{equivalent}	Measured		Simulated		χ^2
			HVL	QVL	HVL	QVL	
34	33.5	0.0	1.711	3.532	1.713	3.579	0.00009
40	39.4	0.0	2.232	4.750	2.238	4.738	0.00012
46	45.5	0.0	2.779	5.978	2.787	5.978	0.00005
49	48.4	0.0	3.060	6.619	3.063	6.578	0.00006

Table 2. Comparison of the measured and simulated attenuation data for a Mo-target tube filtered with 1 mm Al

nominal kV	kV _{equivalent}	Al _{equivalent}	Measured		Simulated		χ^2
			HVL	QVL	HVL	QVL	
22	21.1	0.075	0.388	1.285	0.385	1.286	0.00007
28	28.0	0.100	0.538	1.844	0.540	1.841	0.00005
34	35.0	0.050	0.607	2.050	0.609	2.197	0.00009
40	39.4	0.100	0.654	2.420	0.649	2.442	0.00070
46	45.4	0.150	0.698	2.734	0.686	2.736	0.00071
49	49.0	0.175	0.739	2.907	0.703	2.911	0.00422

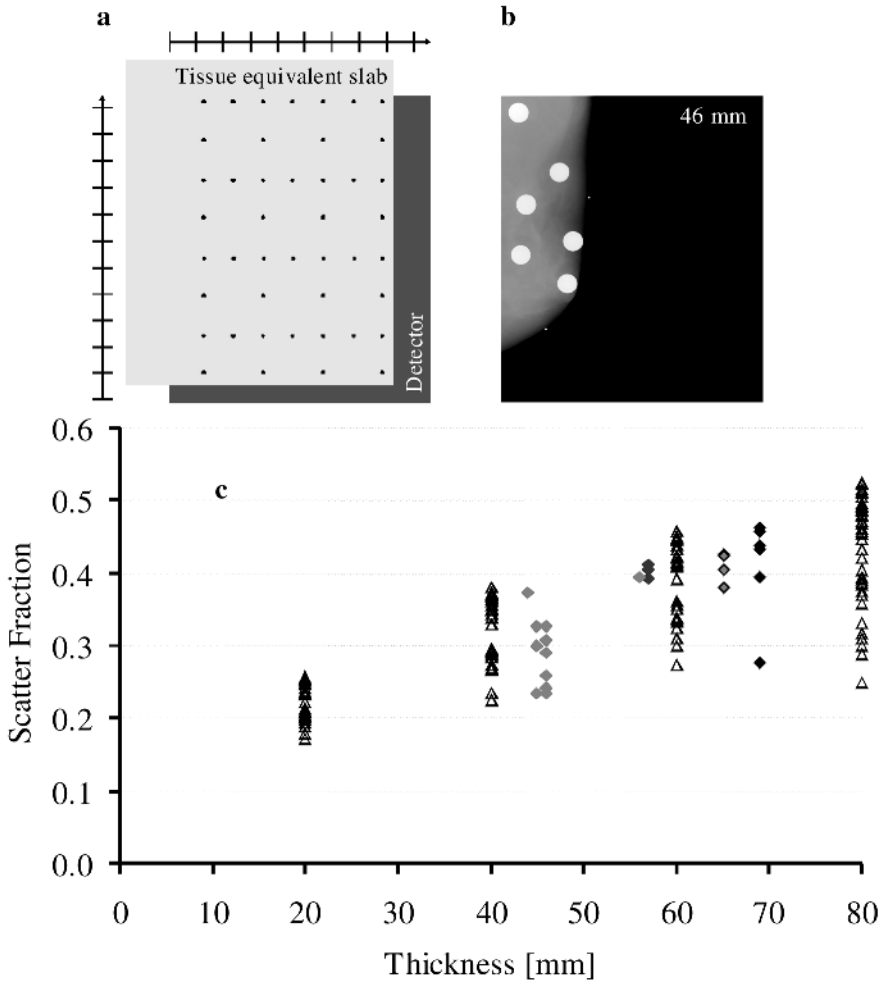


Fig. 1. (a) Geometry of the scatter measurements; 50% glandular, 50% adipose breast equivalent phantoms were used. The black dots indicate the positions where SF were measured. The distance between the ticks on the horizontal and vertical rulers is 2 cm. (b) Image of 12 mm diameter Pb-disks exposed on top of a breast in the MLO position. Breast thickness is shown in the upper right corner. (c) SF as a function of breast thickness in 0° projection images of 50% glandular-50% adipose breast equivalent phantoms (open triangles) and six clinical breast images (solid diamonds).

Shown are $kV_{\text{equivalent}}$ and $Al_{\text{equivalent}}$ of the simulated spectra for a nominal kV that results in the smallest χ^2 . The measured and simulated estimates of the HVL and QVL are also presented. The simulated values are those that minimize the χ^2 . The results in both tables demonstrate that the extrapolation of the Boone’s spectral models agree well with our measurements.

3.2 Scatter

Figure 1a and b show the geometry used for the scatter measurements in the breast tissue-equivalent phantoms and in the patient data. Using the method of extrapolating the SF to zero disk diameter in breast equivalent phantoms demonstrates that scatter fraction increases with thickness, as expected. We measured SF = 0.29 for a 20 mm phantom, 0.43 for a 40 mm phantom, 0.52 for a 60 mm phantom, and 0.57 for a 80 mm phantom as measured near the center of the phantom.

Figure 1c illustrates SF derived from the shadows under 12 mm Pb-disks as a function of breast thickness. The SF correspond to the various positions in the field of view as indicated in Fig 1a and b. This analysis shows that the SF in real mammograms are similar to the SF measured in breast-equivalent phantoms for corresponding thicknesses.

Figure 2 shows the extent to which the iodine concentration will be underestimated if a correction for scatter is not applied. The amount by which the iodine concentration will be underestimated is dependent upon the breast thickness. Consider, for example, the situation were the breast has an actual iodine concentration of 2 mg/cm². Failure to correct for scatter will result in an error in the estimated iodine concentration of 29% for a 20 mm thick compressed breast and 50% for a 80 mm thick compressed breast. Note that even if images are produced with a grid, the iodine concentration is still underestimated. This has relevance for those attempting to perform contrast-enhanced digital mammography.

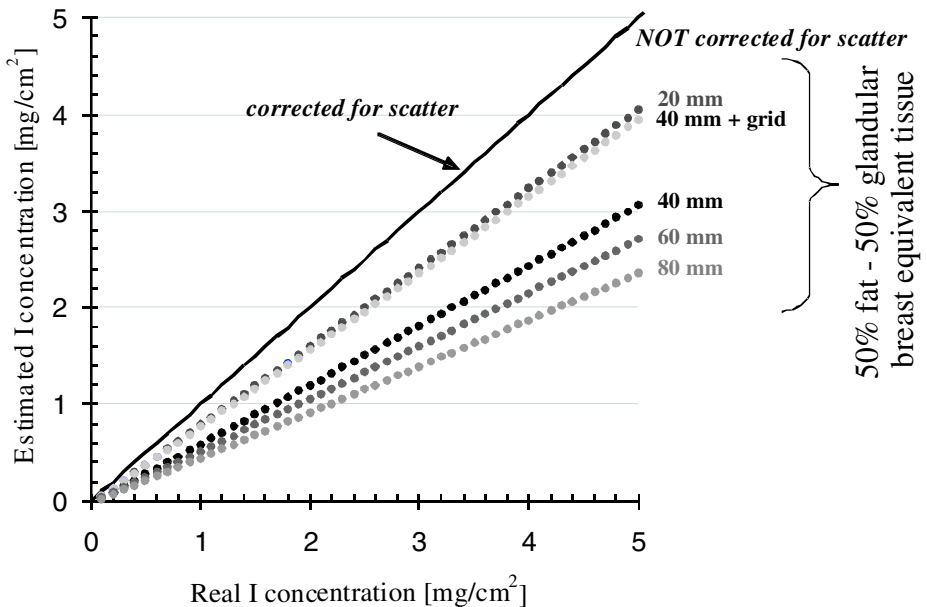


Fig. 2. Iodine concentration will be underestimated if not corrected for scatter. The simulation used a Rh target, 49 kV and 0.27 mm Cu filter. No grid was used if not specified.

3.3 Patient Motion

Figure 3 shows a clinical example of patient motion. The image was produced by subtracting a post-contrast reconstructed image of the breast from a pre-contrast reconstructed image. Two lead BBs are shown attached to the skin near the nipple. The arrows indicate patient motion. In our clinical trial, we consistently noted the greatest motion in the dependent (lower) portion of the breast.

We have attempted to estimate the magnitude of motion artifacts by simulating breast motion. Figure 4 illustrates the influence of displacements simulating patient motion on the relative SI variation and equivalent iodine concentration. The data were calculated from images of 12 women. As an example, 25% of the 6 mm displacements have on average a 1% relative SI variation; this corresponds with a 0.5 mg/cm^2 iodine uptake. However, it is relevant to note that a displacement of as little as one pixel can result in more than a 5% change in signal intensity, which can potentially exceed the anticipated signal from the iodine contrast agent. As such, it is imperative that motion be minimized.



Fig. 3. Example of patient motion

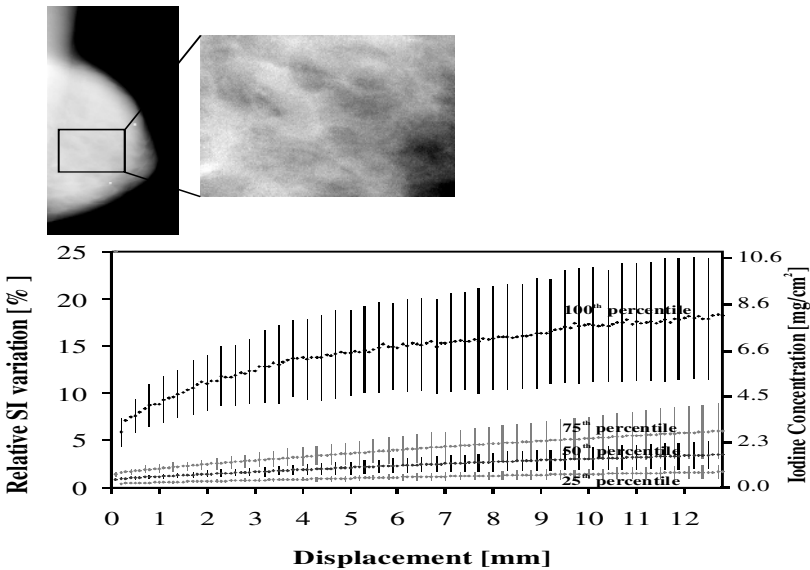


Fig. 4. Example of a ROI extracted from a projection mammogram acquired with a Rh-target x-ray tube at 49 kV with 0.27 mm Cu filtration (left). Relative SI variation between pixel displacements and the corresponding equivalent iodine concentration from 12 projection images are shown (below). The error bars represent standard deviations.

4 Conclusion

CE-DBT offers the potential to visualize the vascular characteristics of breast lesions as an adjunct to mammography. Based upon our initial clinical experience, and the work reported here, it is clear that the quantization of the iodine uptake for CE-DBT is complex. For the design of a CE-DBT system, attention should be paid to scatter and patient motion. At the current time, we are working on the reduction of patient motion and we are evaluating alternative subtraction methods using dual energy CE-DBT. We expect that these may minimize patient motion artifacts.

Acknowledgements

This work was funded in part by NIH grant PO1 CA85484 and a Philips Medical Systems/RSNA Research Seed Grant.

References

- [1] Carton A-K, Li J, Albert M, *et al.* Quantification for contrast-enhanced digital breast tomosynthesis. In: Flynn MJ, Hsieh J, editors. *Medical Imaging 2006: Physics of Medical Imaging*; p. 111-121.
- [2] Jong RA, Yaffe MJ, Skarpathiotakis M, *et al.* Contrast-enhanced digital mammography: Initial clinical experience. *Radiology* 2003;228:842-850.
- [3] Skarpathiotakis M, Yaffe MJ, Bloomquist AK, *et al.* Development of contrast digital mammography. *Medical Physics* 2002;29(10):2419-26.
- [4] Maidment ADA, Adelow L, Blom O, *et al.* Evaluation of a Photon-Counting Breast Tomosynthesis Imaging System. In: Flynn MJ, editor. *Physics of Medical Imaging, Proc. SPIE 6142*; 2006.
- [5] Wu T, Moore RH, Rafferty EA, *et al.* Breast tomosynthesis: Methods and applications. In: Karellas A, editor. *RSNA Categorical Course in Diagnostic Radiology Physics: Advances in Breast Imaging - Physics, Technology, and Clinical Applications*; 2004. p. 149-163.
- [6] Dobbins JT, 3rd, Godfrey DJ. Digital x-ray tomosynthesis: current state of the art and clinical potential. *Physics in Medicine & Biology* 2003;48(19):R65-106.
- [7] Niklason LT, Christian BT, Niklason LE, *et al.* Digital tomosynthesis in breast imaging. *Radiology* 1997;205(2):399-406.
- [8] Boone JM, Fewell TR, Jennings RJ. Molybdenum, rhodium, and tungsten anode spectral models using interpolating polynomials with application to mammography. *Medical Physics* 1997;24(12):1863-74.